

1 **Development and validation of a numerical model for the simulation** 2 **of high velocity impacts on advanced composite armor systems.**

3 Giovanni Sabadin, Marco Gaiotti, Cesare M. Rizzo

4 Marine Structures Testing Lab, DITEN, University of Genova, Genova, Italy

5 Via Montallegro 1, I-16145 Genova (Italy)

6 Alessio Bassano

7 OTO Melara a Finmeccanica company

8 Via Valdilocchi 15, I-19136 La Spezia (Italy)

9 Tel. +39 0103532272

10 E-mail: giovanni.sabadin@gmail.com; cesare.rizzo@unige.it; marco.gaiotti@unige.it

12 **Abstract**

13 The anti-ballistic properties of a new advanced composite armor system have been investigated with
14 the aim to minimize the armor system total weight per unit area. The innovative protection, made of
15 a silicon carbide ceramic outer layer and an inner composite back-packing layer formed by ultra-high
16 molecular weight polyethylene (UHMWPE) fibers, namely Dyneema[®] Hard Ballistic 26, was
17 realized and then tested performing dedicated ballistic impact tests.

18 In order to investigate its permanent deformation, ceramic cracking, dimension of the rupture and
19 extension of the impact damage, non-destructive and destructive tests were conducted on the tested
20 panels. The experimental results were used to develop and validate a transient non-linear dynamic
21 simulation model of the high velocity impact of a 7.62 AP bullet on the tested armor system. After
22 an accurate setting of the parameters involved in the description of the material constitutive models
23 and of the involved physical phenomena, a complex numerical model was developed in the ANSYS-
24 Autodyn[®] environment using both mesh and meshless approaches at the same time. The comparison
25 reveals a good agreement between experimental and computational results in terms of ballistic

26 properties, deformations, fragmentation and fracture of the ballistic armor system. Hence, a new
27 numerical model for the design and the optimization of the ballistic efficiency of composite armor
28 systems was developed and can be now used in current practice.

29 **Keywords:** high velocity impact, composite, multi-layer, armor system, ballistic tests, numerical
30 simulation

31 **1 Introduction**

32 The application of advanced composite materials in the development of armor systems is well
33 established. Compositions of novel materials are particularly suitable for the integration and
34 improvement of ballistic protections in key sectors of the defense industry, especially in the
35 automotive, aeronautical and more recently in the shipbuilding industry. The significant reduction of
36 the total armor weight obtained by the use of these new materials in lieu of traditionally hard steel
37 protections made by Rolled Homogeneous Armor Steel (RHA) is well known (Fecko, et al., 2005).
38 The reduction of total armor weight generally leads to an increase of the vehicle performance in terms
39 of speed and maneuverability: this means the improvement of the survivability of the vehicle and the
40 protection of the crew members in a combat situation.

41 Actually, the new advanced composite armors (ACA) are built up by different multi layers materials
42 in order to guarantee the ballistic protection at different levels of threats as described e.g. in standards
43 like the NATO-STANAG – 4569 (NATO, 2004) or the U.S. NIJ Standard 0108.01 (National Institute
44 of Justice, 1985). For relatively weak threats, a suitable number of single layers of fiber-reinforced
45 polymer-matrix composite is sufficient, see e.g. (Grujicic, et al., 2008) (Lim, et al., 2003). When
46 increasing the threats, it becomes necessary to develop a combination of different materials in order
47 to guarantee the ballistic protection (Ramadhan, et al., 2012) (Flores-Jhonson, et al., 2011).
48 Nowadays, best innovative solutions and lighter armor systems are made up of an outer layer of
49 ceramic materials and a back-packing in fiber-reinforced polymer-matrix. In fact, the ability of a
50 composite armor to provide useful contribution to an impact event depends on the hardness of the
51 ceramic materials, which is critical for blunting and eroding the projectile, and the strain to failure of

52 the fiber-reinforcement, which determines the ability of those materials to absorb kinetic energy via
 53 a global deformation process. Different ceramic materials can be adopted in the form of ceramic tiles
 54 in the protections such as Alumina (Al_2O_3), Silicon Carbide (SiC), or Boron carbide (BC): density
 55 and properties of the ceramic vary proportionally to their cost. Only when an extremely low weight
 56 is required, expensive SiC and BC tiles are used.

57 For the back-packing layers, different innovative fibers can be applied such as, polypropylene fibers
 58 (e.g. Tegirs[®]), aramidic fibers widely known as Kevlar[®] and, more recently, a new composite
 59 material made of Ultra High Molecular Weight Polyethylene (UHMWPE) fibers, very suitable to
 60 absorb the energy of a ballistic impact. These innovative fibers, commercialized in the late 1970 under
 61 the trade name Dyneema[®], have densities less than water ($0,97 \text{ kg/m}^3$) and high tensile ultimate stress,
 62 in excess of 3GPa (Karthikeyan, et al., 2013). Their very high specific strength and stiffness led to
 63 their use in many different fields like e.g. high performance sails, fishing lines and marine mooring
 64 cables; woven fabrics are used to make protective gloves.

FIBRE	ρ (kg m ⁻³)	$\dot{\epsilon}$ (s ⁻¹)	σ_f (GPa)	ϵ_f (%)	C^* (ms ⁻¹)
Dyneema [®]	970	700	2.55	6.26	698
Spectra 900	970	433	2.5	3	689
M5	1700	Not stated	4	1.4	712
Toray T1000	1800	Not stated	6.4	2.2	947
Toray T700	1570	1000	3.4	1.57	665
Kevalr 49	1440	1350	3.08	3.86	650

65 *Table. 1 Values of the density ρ , tensile failure strength σ_f and the failure strain ϵ_f measured at the strain*
 66 *rate $\dot{\epsilon}$ and the corresponding value of the Cunniff velocity C^* (Russel, et al., 2013)*

67 Since the initial numerical study on the ballistic performances of laminates reinforced by UHMWPE
 68 fiber as reported by (Frissen, 1996), it was noted that the mechanical properties are competitive for
 69 ballistic and blast applications. Nowadays, it is well known that the hard ballistic Dyneema[®]
 70 guarantee excellent protection against threats and fast-moving Improvised Explosive Device (IED)
 71 fragments. As reported in (Russel, et al., 2013), and namely from the value of the mechanical
 72 properties reported in Table 1, it is clear that UHMWPE fibers are very competitive for ballistic and
 73 blast application. Cunniff defined the velocity C^* (Cunniff, 1999) that express the ballistic

74 performance of the fibers in terms of maximum bullet velocity. At the same time, the UHMWPE
75 density is considerably lower with respect the other fibers having similar ballistic performances, not
76 to mention metallic materials. Published data on Dyneema® are very scattered and the first
77 characterization of the dynamic behavior of a Dyneema® composite is rather recent in relevant
78 literature, see (Iannucci, et al., 2009), (Grujicic, et al., 2008). Only in recent years, the research
79 focused extensively on the description of the dynamic behavior and properties of such materials in
80 order to extend material models to armor-grade composite materials. The main contributes derive
81 from the research of (Russel, et al., 2013), (Karthikeyan, et al., 2013) and (Lassig, et al., 2015). Very
82 recent research focuses on the penetration mechanism of a steel sphere onto composite armor systems
83 made by Dyneema® Hard Ballistic 26 as presented in (O'Masta, et al., 2014). The definition of a high-
84 fidelity material model moves the challenge in the dynamic numerical simulation of the High Velocity
85 Impact (HVI) of the bullet into the advanced composite target using dynamic phenomena simulation
86 software like e.g. Ls-Dyna®, Abaqus® or ANSYS-Autodyn®. Indeed, the possibility of properly
87 simulating the bullet impact onto a composite armor system is very useful to optimize layers' types
88 and thickness and consequently to minimize the total weight of the protection without the need of
89 rather expensive and complex experimental tests.

90 The lack in literature of research focused on the impact simulation of 7.62 AP bullet on a composite
91 armor system made of a ceramic layer and a back-packing of UHMWPE fiber reinforced laminate
92 moves the present study. In order to obtain a reliable numerical model, an intensive study was carried
93 out comparing the experimental results of ballistic impact tests with the numerical results derived
94 from simulations developed in the frame of a research project cooperation. The developed anti-
95 ballistic solution applies advanced materials with high technological content and the most recent
96 techniques for lamination and bonding. The created panel is a real innovation in the field of vehicle
97 ballistic protection and even more in the defense systems, leading to significant savings in terms of
98 total weight of the protection.

99 The request to develop and validate an innovative numerical model to simulate the impact of a bullet
100 upon an add-on composite armor system was the challenge of the research involving the Italian
101 company OTO Melara and DITEN of the University of Genova. The model was intended for patrol
102 boats, finally aimed at minimizing total weight of the armor system but still securing a specific
103 protection level and additionally withstanding the harsh marine environment. To guarantee the
104 maximum reduction of the add-on protection weight, remarkable importance was paid to the
105 application of innovative anti-ballistic materials and to their cost. After a first literature review and
106 taking advantage of the know-how of OTO Melara, it was eventually decided to develop a new armor
107 system made by a first layer of SiC ceramic glued onto a back-packing made of UHWMPE laminate.
108 Next, the initial development and validation of a numerical model of the projectile penetration into a
109 target armor system (Sabadin, et al., 2014), it was decided to improve and validate a new numerical
110 model that allows obtaining impact behavior of a ballistic protection made of SiC ceramic and
111 UHWMPE fibers. Due to the lack of experimental and numerical results in literature concerning this
112 impact typology, actually needed for a comparison with further numerical results, it was necessary to
113 plan the realization of the add-on panels and the execution of dedicated ballistic test in order to obtain
114 experimental results for model validation. After conducting the experimental campaign and
115 evaluating the anti-ballistic capacity of the new armor system, an enhanced numerical model was
116 developed through the implementation of “hydrocodes”, i.e. software particularly suited to model
117 HVI, bullet penetration and blast events, simulating the tridimensional configuration of the bullet
118 impacting upon the panels.

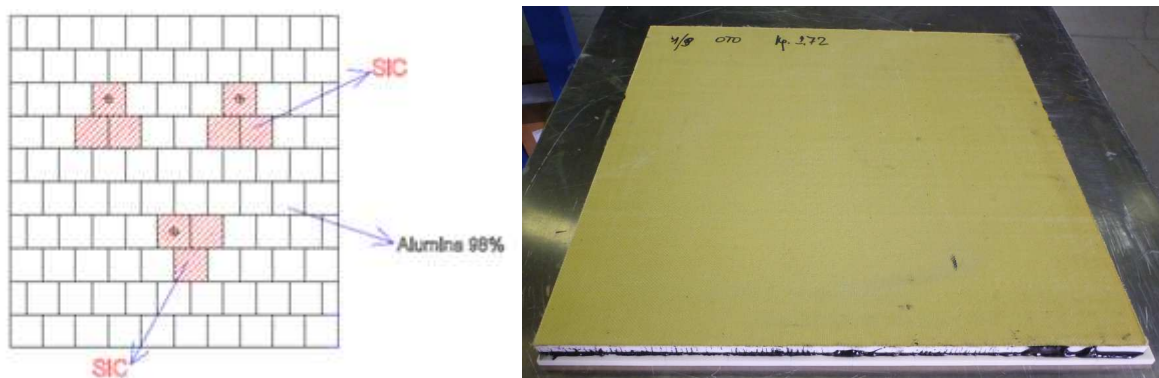
119 In the present paper, a complete description of the test cases as concern geometry, adopted material,
120 construction method and final dimension of the armor system is presented at first. Then, the required
121 standard threat levels and the conducted ballistic impact tests are described. The destructive and non-
122 destructive tests on the impacted specimens, including analysis of images of the damage and
123 dimensions of the fracture for the different materials are thereafter discussed. The definition of the
124 numerical model, the calibration of the main parameters of the simulation software as well as the

125 related investigations about the physics of the phenomena are subsequently reported, particularly
126 referring to the dynamic characterization of the material constitutive models for the UHMWPE fibers.
127 Finally, comprehensive comparisons between the numerical simulation results and the experimental
128 impact tests ones are reported, eventually validating the numerical model. Appositely hidden results
129 are reported due to obvious confidentiality reasons.

130 **2 Tests description**

131 **2.1 Armor system**

132 For the ballistic impact tests, a rectangular add-on panel system has been realized in order to guarantee
133 the fourth protection level (named Armor-Piercing Rifle) as defined by the NIJ Standard 0108.01
134 (National Institute of Justice, 1985). Here, the level of threat considered is a 30-06 M2 Armour
135 Piercing (AP) bullet. Fig. 1 shows one of the tested specimens.



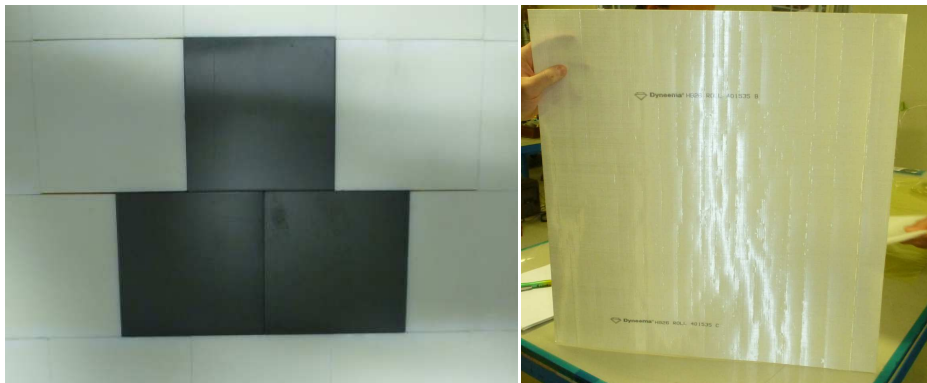
136

137

Fig. 1: Geometry of the tested panels.

138 The panels have square shape; they consist of a first outer layer made of ceramic tiles with high
139 strength and hardness proprieties and a second back-packing layer made of high modulus fiber
140 composite, each layer is bonded to the other by a glue specifically produced for these assemblies.
141 Each specimen was made to ensure the possibility of carrying three different impacts of a projectile
142 in three distinct areas: the ceramic tiles material are positioned as shown in Fig. 1. Only nine tiles in
143 the specimens were made by the rather expensive ceramic material selected for the composite armor
144 system while cheaper Alumina 98% tiles were used for the remaining of the panel as usual in similar
145 cases. In particular, the armor ceramic tiles used in all the tested panels as shown in Fig. 1 are Silicon

146 Carbide (with a relatively low density of $3,15 \text{ g/cm}^3$ and a very high elastic modulus of about 410
147 GPa. The back-packings are made by an UHMWPE Dyneema® Hard Ballistic 26; these fibers are
148 characterized by higher impact and fatigue strength compared to other ballistic materials as shown in
149 Table 1. See Fig. 2.
150 Impacts are aimed at the SiC tile center, thus ensuring ballistics impacts comparable with those made
151 by numerical simulation.



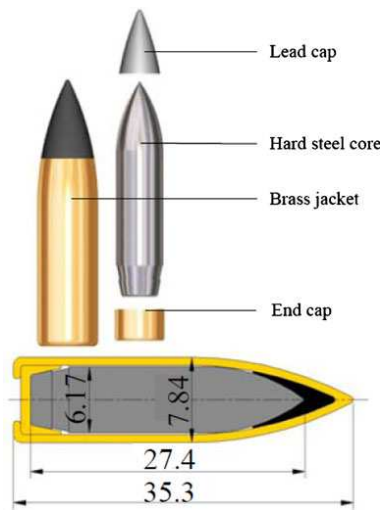
152
153 *Fig. 2: Materials used in the panel: a) tiles of Silicon Carbide; b) single layer of Dyneema® Hard Ballistic*
154 *26.*

155 Each individual fabric layer has an areal density ranging between $257\text{-}271 \text{ g/m}^2$; for convenience it
156 is therefore considered an average density of the layers of 262 g/m^2 and each layer has an average
157 thickness of 0.38 mm. The armor total thickness is less than 20 mm but for confidentiality reasons
158 this paper omits the actual thickness of the layers. These advanced materials allow containing the
159 total areal density of the protection with respect to other antiballistic solutions commonly installed
160 on land vehicles: in fact the total areal density of the described add-on panel is 35 kg/m^2
161 approximately, while a value of about 40kg/m^2 is the standard.

162 **2.2 Cartridge 30-06 M2 SPRG description.**

163 The threats used for the ballistic tests are the cartridge caliber 30-06 M2 SPRG. This bullet is
164 commonly called M2 Armor Piercing bullet and is identified by the black color on its front; also, the
165 total length of the cartridge is 63.2 mm. The bullet inside the cartridge is composed by three different
166 materials: an outer jacket made of cart brass, an internal core of hard steel and the rear part in lead.
167 The total weight of the bullet is 10.53 g and the average total length is 35.3 mm. The dimensions

168 shown in Fig. 3 represent the average size of the projectile of the cartridge in the manufacturing phase.
169 Actually, these dimensions may have 0.01 - 0.02 mm deviations due to the manufacturing process.



170
171 *Fig. 3: 30-06 M2 bullet from (Forrestal, et al., 2010), measures in mm*

172 The bullet is fired at an average speed of 868 m/s, thus constituting a significant threat in the field of
173 projectiles having 7.62 caliber.

174 **2.3 NIJ -0108.1 Standard and test set up**

175 US NIJ Standard-0108.01 Ballistic Resistant Protective Materials establishes five degrees of threat
176 based on caused damage, and then provide the appropriate standard level of protection (National
177 Institute of Justice, 1985). The standard was drafted to describe and share different types of
178 configurations for bulletproof vests.

179 The protection level required in the frame of this research is the type IV (Armor-Piercing Rifle),
180 where the reference ammunition for the qualification is the Armor Piercing 30-06 M2 with a total
181 mass of 10.8 g and an impact velocity of 868 +/- 15 m/s. This level of threat depicts the bullet impact
182 used by sniper rifles against the target: the high internal energy of the projectile, the geometry itself
183 of the ogive and the materials make this ammunition the most lethal threat taken into consideration
184 by the US Standard.

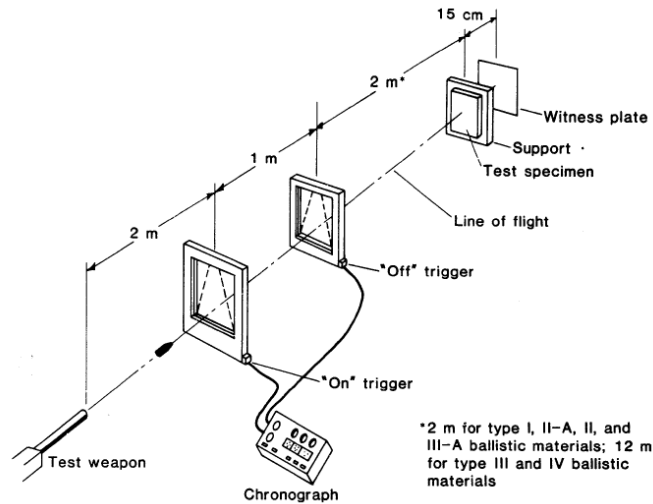


Fig. 4: Setting ballistic tests (National Institute of Justice, 1985)

185
186

187 The technical specification indicates to hit each panel with three separate shots; each single shot must
188 hit a single area of SiC tiles. The impact at the center of the tile will be useful to obtain an experimental
189 comparison for the numerical simulations.

190 The ballistic tests are performed according to Fig. 4: each panel is tested individually, repeating the
191 operations for each of the three targets on the panel.

192 The test needs a few elements to be performed, besides many safety and security issues:

- 193 ✓ A test manometric barrel suitably supported to hit the targets in the selected points also
194 analyzing temperatures and gases produced by the explosion.
- 195 ✓ Between the barrel and the target an optical barrier is placed allowing the precise and reliable
196 determination of the speed of the projectiles, ranging from 500 to 1000 m/s (an averaged value
197 of 868 m/s was used in computations).
- 198 ✓ At a predetermined distance from the barrel, the target is placed on a support structure (Fig.
199 5), to constrain the panels. For these experimental tests, the panel is fixed only on the edges,
200 leaving free the central part where the impact takes place.



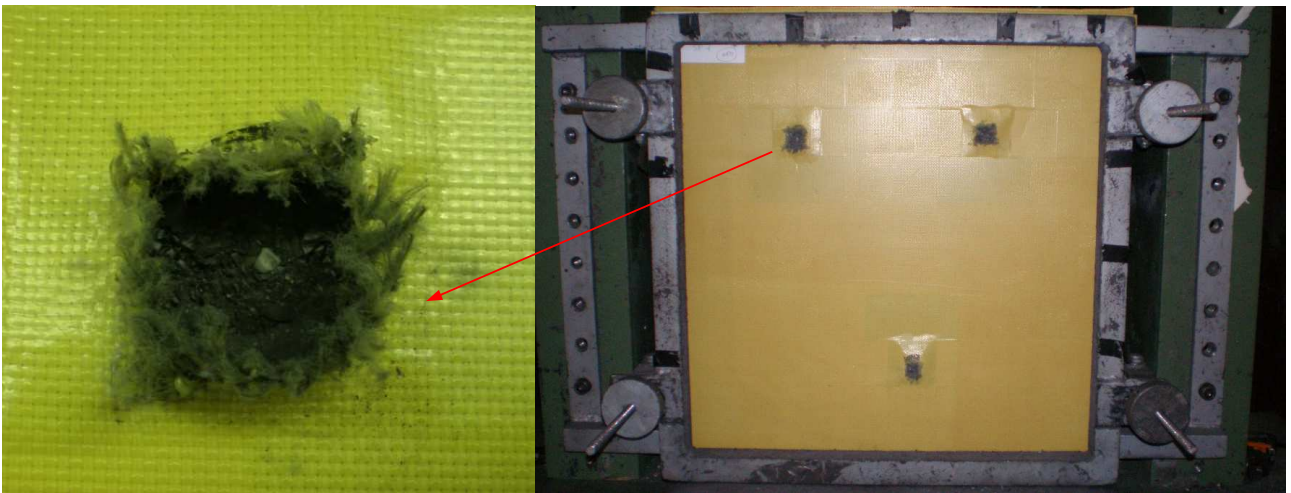
201
202

1
Fig. 5: Rigid structure for fixing the target panel edges.

203 **3 Experimental results**

204 **3.1 Ballistic impact results**

205 On each panel three M2 bullets were fired in points marked in correspondence of the SiC tiles, see
206 Fig. 6.



207
208

Fig. 6: Strikes on tested panel

209 In Table. 2 the results of the experimental tests are summarized: the panel protected by SiC tiles
210 proved suitable to ensure the ballistic protection for the selected threat level.

211 Among nine impact tests performed on three panels, only one shot completely perforated the panel
212 (CP, Complete Penetration) while the other 8 shots were hold by the armor. It was therefore decided
213 to validate the full protection provided by the panel, having obtained a protection with an areal density

214 of 35 kg/m² able to prevent perforation to a threat of NIJ Grade IV. It is worth again noting that a
 215 saving in weight of 15-20% compared to conventional reinforcement in composite armors as reported
 216 in the literature has been obtained (see e.g. (Hogg, 2003)).

PANELS	PANEL n°	IMPACT	RESULTS
SiC-HB26	PANEL 1	TEST 1	CP
		TEST 2	H
		TEST 3	H
	PANEL 2	TEST 1	H
		TEST 2	H
		TEST 3	H
	PANEL 3	TEST 1	H
		TEST 2	H
		TEST 3	H

217 *Table. 2 Experimental results and damage caused by the shot (CP=complete penetration, H=hold)*

218 One panel was tested with the presence of a clay layer in the back of the target in order to evaluate
 219 the dynamic damage effect of the impact. This makes possible to assess the actual deflection
 220 extension of the dynamic impact suffered by a rear structure.



221
 222 *Fig. 7: Impact test with modelling clay on its rear.*

223 The test effect on the clay, shown in Fig. 7, is represented by the penetration of the panel inside the
 224 clay layer in the shape of three spherical recesses. It was then measured the maximum penetration for
 225 each impact inside the clay by a digital caliper, the penetrations were measured in the range of 30
 226 mm.

227 **3.2 Specimens examinations**

228 Once completed experimental tests, the panels became the subject of non-destructive and destructive
229 analyses aimed at obtaining the characterization of the different types of damages and fractures due
230 to the impact into ceramic materials and into back-packing. These analyses also allowed displaying
231 and defining the actual mechanism of penetration of the projectile inside the composite material.

232 At first, each specimen was firstly subjected to radiographic analysis aimed at obtaining the size of
233 the holes of the projectile, the breakage of the small panels of ceramic material, the propagations of
234 the fractures within the ceramic material and the fragmentation of the projectile. In addition, for each
235 tested panel a three-dimensional scan of the external geometry was performed, from which the
236 detailed extent of the damage and the total deflection of the bulge of the panel back side are obtained,
237 assessing quite accurately the effect of the impact of the bullets.

238 Once concluded the non-destructive analysis on individual panels, at the Marine Structures Testing
239 Lab of DITEN all destructive analysis were conducted with the purpose of obtaining further
240 information about the kinds of fractures and on their propagation within the various materials and
241 also to visually confirm the non-destructive evaluations about the penetration of the projectile inside
242 the panel.

243 **3.2.1 Radiographic analysis**

244 The X-ray analyses allow evaluating the structural integrity of each tile of ceramic material and in
245 particular to verify the breakage and fracture propagation after the bullet impact, during the ballistic
246 tests. However, a limitation of the radiographic analysis was due to the presence of the ceramic layer
247 itself on the panels: as a matter of facts, the evaluation of the delamination phenomena on the rear
248 Dyneema® back-packing was not possible. Nevertheless, this analysis allowed verifying, with
249 significant accuracy, the penetration hole size of the projectiles, the breakage of the ceramic tiles and
250 the propagation of the fractures inside the adjacent tiles. In all radiographs, whose Fig. 8 is an
251 example, the following types of damages can be displayed and highlighted:

- 252 ✓ Fragmentation of the central core of the projectile and dispersion of the fragments, a
253 phenomenon greatly highlighted by the presence of a clearer "cloud" in the images, which
254 defines in fact the propagation of fragments and steel powders of high density as far as an
255 increased absorption of the X-ray is caused by the higher density of the material;
- 256 ✓ Complete rupture of the ceramic tiles on which the impact takes place, evidenced by the more
257 definite color of the tile and by the presence of small size fragments;
- 258 ✓ Damage propagation on adjacent tiles (including white Alumina tiles);



259
260 *Fig. 8: Panel radiography, complete brake and fragmentation of the Sic tile impacted*

261 X-ray images obtained were later compared with the pictures obtained from the destructive tests of
262 the panels: the comparison is useful to support and complete the analyses of some cases difficult to
263 be interpreted.

264 3.2.2 Tri-dimensional scan

265 The extension of the panel maximum back-packing deflection in way of the bullet point of impact
266 and the extension of the damage areas on front and rear surfaces for each point of impact appear to
267 be of paramount importance for the comparison between the ballistic tests results and the numerical
268 simulations. The panels were then scanned to provide information necessary for the comparison.
269 Accurate geometry of each tested specimen was obtained by means of a three-dimensional scanner
270 without any contact possibly affecting the surface shape, see Fig. 9. A CAD model was obtained
271 where the scan information is summarized and stored.

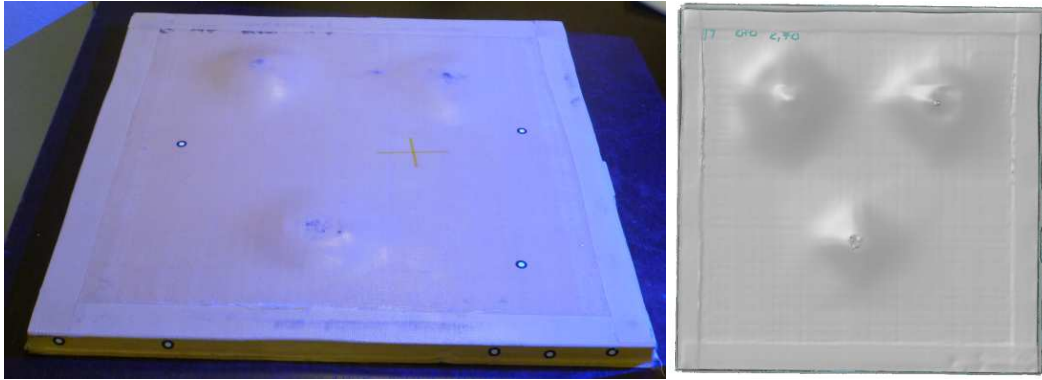


Fig. 9: Acquisition of three-dimensional scans

272
273

274 Taking advantage of the accurate CAD model of the scanned surfaces, quantitative information were
 275 gained such as the maximum extension of the residual rear deflection in way of the bulge, the
 276 deformation of the front surface of the panel, the different shapes and sizes of the damaged areas (Fig.
 277 10).

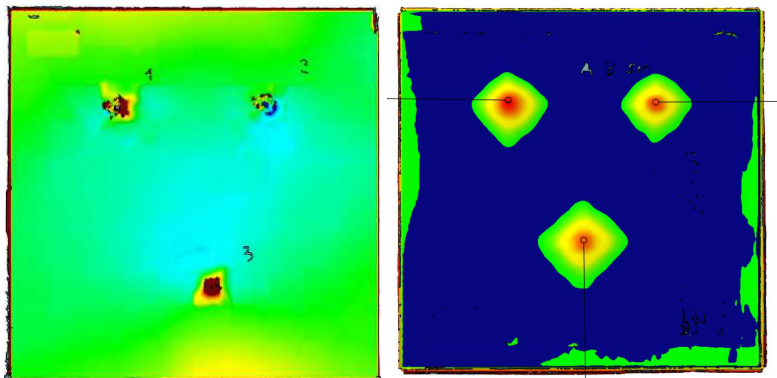
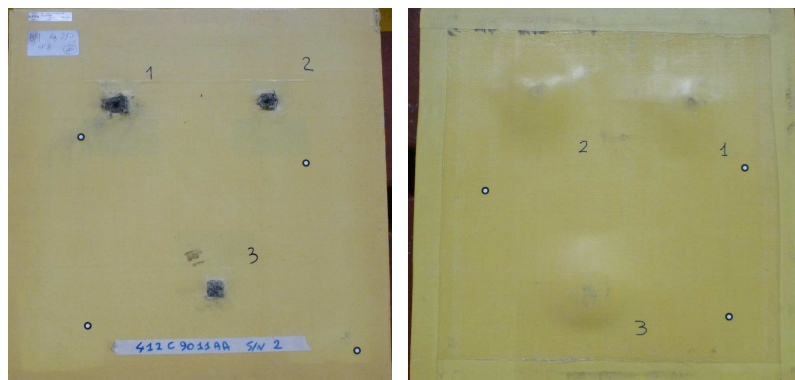


Fig. 10: Tri-dimensional scan of the impact target (front and rear).

278
279

280 3.2.3 Destructive analyses

281 All the observations made during the phases of destructive analysis conducted at the DITEN Marine
 282 Structures Testing Lab are described in the following. They allowed evaluating and defining the size
 283 of the different types of damages and fractures occurred in the material.



284

285

Fig. 11: Front and rear of a tested panel before destructive tests

286 The tested panels have been subject to a detailed photographic analysis of the damage extension due
 287 to the bullet impact on the back surface and the front plate before any destructive analysis (Fig. 11).
 288 The main damage dimensions measured during the non-destructive analyses were also confirmed for
 289 each point of impact from photos and direct measurements as reported in Table 3. The results reported
 290 are normalized with respect to the real dimension of the square ceramic tiles due to confidentiality.

Main dimension holes								
Type	Panel	Shoot n°	Ø holes	Est. Front Damage		Est. Rear damage		RESULTS
				HOR.	VERT.	HOR.	VERT.	
-	-	n°	%	%	%	%	%	
SiC - HB26	412C 9011AA SIN 1	1	44.0%	106.0%	110.0%	154.0%	142.0%	HOLD
		2	38.0%	108.0%	104.0%	174.0%	160.0%	HOLD
		3	46.0%	162.0%	110.0%	154.0%	148.0%	HOLD
	412C 9011AA SIN 2	1	56.0%	108.0%	100.0%	248.0%	238.0%	HOLD
		2	50.0%	80.0%	96.0%	268.0%	288.0%	HOLD
		3	44.0%	100.0%	110.0%	274.0%	256.0%	HOLD
	412C 9011AA SIN 3	1	58.0%	142.0%	132.0%	254.0%	262.0%	Perforation
		2	24.0%	114.0%	144.0%	240.0%	226.0%	HOLD
		3	56.0%	106.0%	112.0%	216.0%	196.0%	HOLD

291

Table. 3 Main dimension of impact holes in the tested panels (normalized)

292 After completely removing the protective top layer, the breaks and fractures involving the ceramic
 293 layers are revealed: Fig. 12 shows images of the interior of a panel with cracks in the SiC tiles: damage
 294 caused by the impact is clearly visible and even the location and extension of the damage over the
 295 entire panel surface.

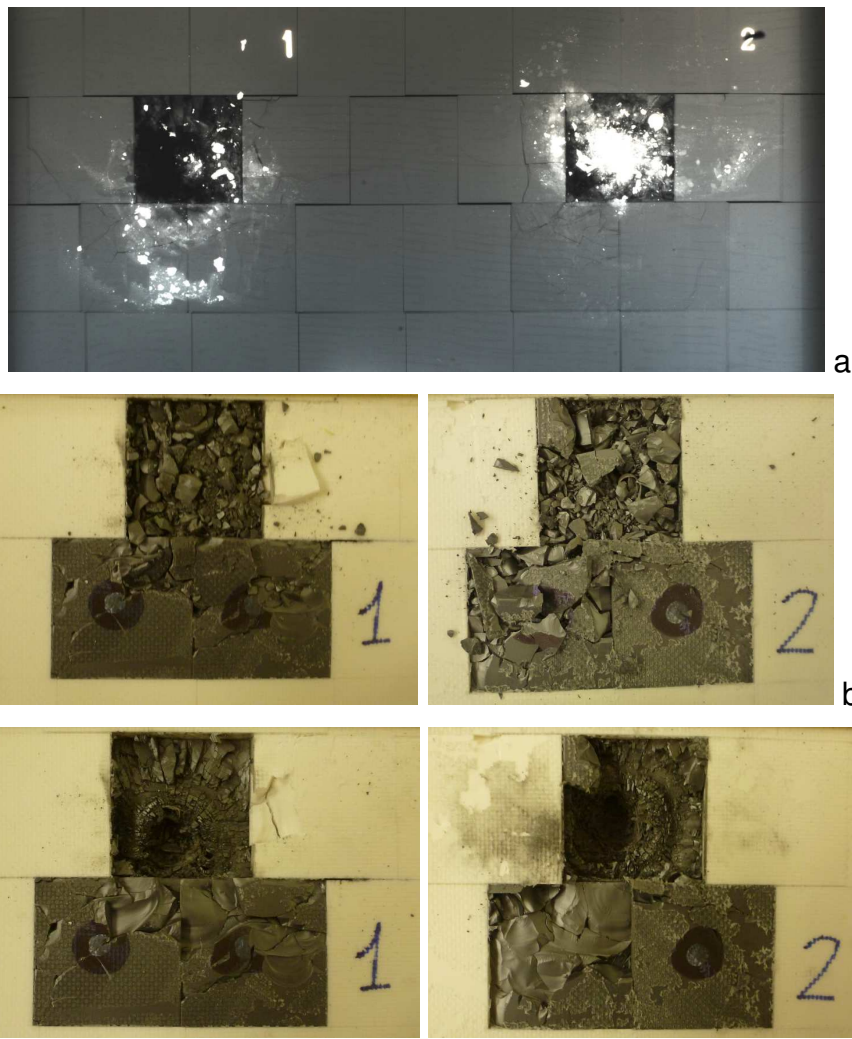


296

297

Fig. 12: Ceramic tiles on the panel after top protection removal

298 Fig. 13 compares the radiographic images with the ones obtained from destructive tests after removal
 299 of the protective top layer. After carefully removing the ceramic debris, the true size of the damage
 300 extension on the impacted tiles appear. The extent of fractures on the impacted tile and on the adjacent
 301 ones allow evaluating the damage propagation and the different type of penetration of the projectile:
 302 the main dimensions of the damage and fracture due to the impact were measured as per Table 4, the
 303 internal penetration of the bullet are referred to the armor total thickness.



304

305

306

307 *Fig. 13: Radiographic analysis (a) compared with real tears with (b) and without (c) ceramic debris. Note:*
 308 *X-ray image from opposite side*

Type	Panels	n° hole	Ø hole	Est. Tiles damage		Est. Fracture propagation		Internal Penetration
				HOR.	VERT.	HOR.	VERT.	
-	-	n°	%	%	%	%	%	%
SiC-HB26	412C 9011AA SIN 1	1	24.0%	142.0%	172.0%	SiC only	SiC only	100.0%
		2	14.0%	154.0%	176.0%	202.00%	SiC only	120.0%
		3	20.0%	150.0%	100.0%	180.00%	SiC only	105.0%

412C 9011AA SIN 2	1	24.0%	202.0%	186.0%	SiC only	SiC only	105.0%
	2	52.0%	150.0%	202.0%	SiC only	SiC only	130.0%
	3	42.0%	100.0%	100.0%	SiC only	SiC only	110.0%
412C 9011AA SIN 3	1	//	1	1	220.0%	200.0%	//
	2	//	1	1	120.0%	200.0%	//
	3	//	1	1	220.0%	140.0%	//

Table. 4 Ceramic layer damage dimension

309

310 The removal of ceramic tiles from the panel allows evaluating and analyzing the deformation of rear
 311 backpacking. It was possible to determine the geometrical dimensions of the extensions of the front
 312 damage and the projectile perforation inside the material, Fig. 14.

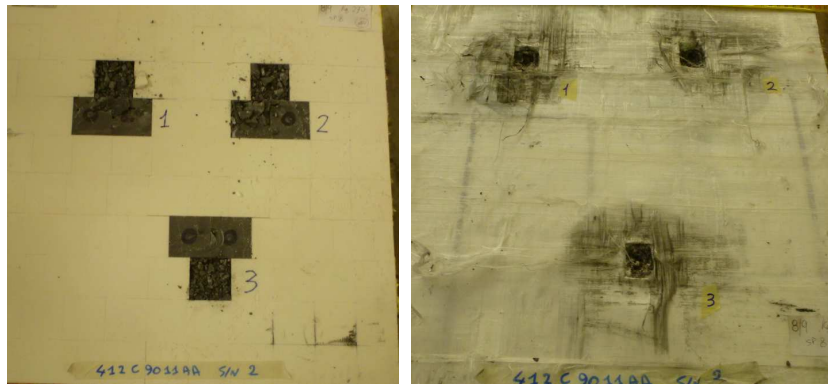


Fig. 14: Front face and rear back-packing surface of a panel

313

314

315 For all the impact points, detailed investigations related to the geometry of the entry wound of the
 316 bullet, the extension of the deflection on the back-packing back and damage the fibers in the area of
 317 impact were carried out. In Fig. 15, two images of the damage caused by the impact of the bullet are
 318 shown: the geometry of the hole is rectangular and the fibers inside the impact hole are burned during
 319 the penetration.

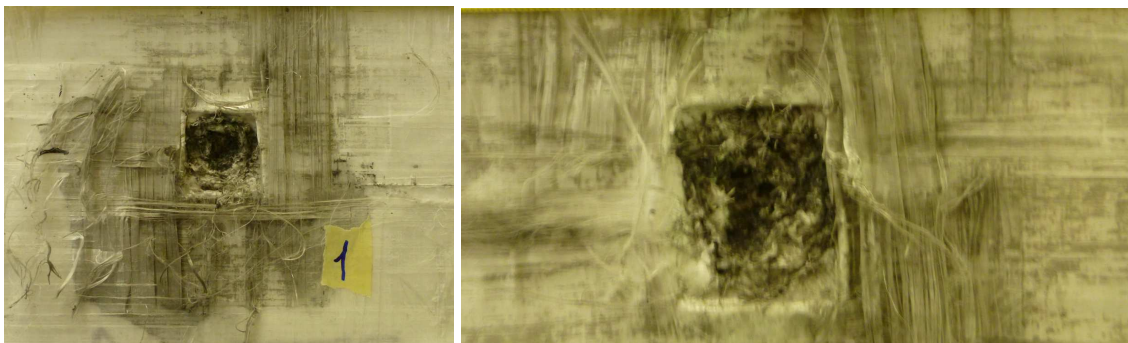


Fig. 15: Impact perforation on back-packing (front and rear sides)

320

321

322 Table 5 shows the main dimensions of the holes referred to the real dimension of the ceramic tiles: in
 323 particular, the vertical and horizontal extension of the penetration damage on the ceramic tiles and
 324 the extension of the damage on the front surface of the panel were carefully measured. In addition to
 325 the hole diameter, also the internal penetration and the real bulging are reported normalized with
 326 respect to the total amour thickness.

327 During the destructive analyses of the impacts on rear backpacking, it was possible to extract, at
 328 impacts not fully penetrated, the central cores of the 7.62 M2 bullets and portions of their outer
 329 covering brass: it is useful the evaluation of the type of fracture and breakage of the projectile during
 330 the ballistic impact. All the bullets were analyzed and results are the starting basis for subsequent
 331 numerical simulations. Fig. 16 shows an example of extracted bullet portions.

Dimensions backpacking Dyneema breaking									
Type	Panel	n° hole	Ø hole	Est. Damage Penetration		Est. Bulge Propagation		Internal	Rear
				HOR.	VERT.	HOR.	VERT.	Penetration	Bulging
		n°	%	%	%	%	%	%	%
SiC- HB26	412C 9011AA SIN 1	1	26.0%	52.0%	60.0%	150.0%	126.0%	100.0%	260.0%
		2	20.0%	52.0%	58.0%	142.0%	130.0%	120.0%	305.0%
		3	18.0%	52.0%	50.0%	144.0%	140.0%	105.0%	250.0%
	412C 9011AA SIN 2	1	30.0%	62.0%	68.0%	238.0%	230.0%	105.0%	410.0%
		2	26.0%	64.0%	76.0%	214.0%	224.0%	130.0%	620.0%
		3	24.0%	62.0%	74.0%	270.0%	204.0%	110.0%	450.0%
	412C 9011AA SIN 3	1	18.0%	66.0%	64.0%	202.0%	196.0%	//	560.0%
		2	12.0%	74.0%	70.0%	216.0%	220.0%	//	470.0%
		3	14.0%	70.0%	60.0%	52.0%	140.0%	//	430.0%

332 *Table. 5 Dimension backpacking Dyneema® breaking*



333
 334 *Fig. 16: Extractions of bullets and their outer coating*

335 From the analysis, actual characteristics of the deformation of the bullet due to the impact are drawn
 336 out as follows:

- 337 ✓ Breaking and brittle deformation of the high strength steel core: all the specimens show
 338 breakage typical of fragile material as expected due to erosion of the bullet.

- 339 ✓ Presence of metal debris from eroded projectile inside the points of impact: all these
340 compounds have a small size of 1-2 millimeters at most.
- 341 ✓ The outer brass is deformed, completely folded back on itself and remains stuck in the panel
342 during the penetration of the projectile.
- 343 ✓ Note the separation of "caps" back of the brass coating that looks undeformed after the impact.

344 **3.3 Ballistic tests summary**

345 During the tests, breaking behavior of the ceramic material was obtained despite its interpretation is
346 rather complex. Moreover, the Dyneema[®] back-packing behavior has been characterized, which was
347 not reported in previous works in open literature to the best of the authors' knowledge; only in
348 (O'Masta, et al., 2014) and (Fallah, et al., 2014) the rupture of Dyneema[®] fibers due to blast or
349 different impact events are indeed addressed. All this information was used to validate the simulation
350 by matching the deformation of the panels and the extension of the damage.

351 3.3.1 Geometry and size of the damage

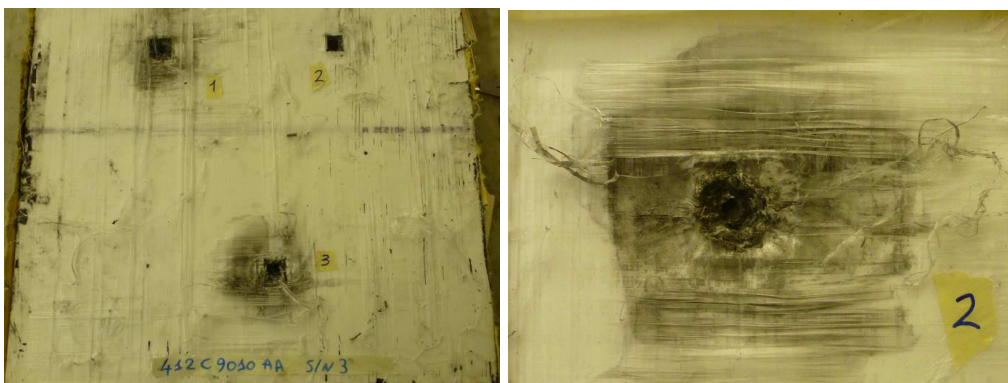
352 The damage generated by the impact of the projectile on the front surface of the panel appears to be
353 limited, well defined and visible; the entry wound of the bullet has a diameter ranging from 1.2 to 2.9
354 mm. In Table 5, the damage parameters are shown.

355 The maximum static deflection detected by the non-destructive analysis highlighted a static bulging
356 up to six times lower than the maximum dynamic deflection imprinted on the layer of clay and due
357 to the dynamic effects of the impact. The average penetration inside the modeling clay of the three
358 perforations was about 30 mm while the panels show a maximum deflection after the test of about 5-
359 6 mm. The effect of the presence of the clay was approximately considered by engineering judgement.
360 This information is very important to estimate the permanent damage generated on the armor
361 protection in comparison to the total elastic one. Moreover, the protected structure laminated or fixed
362 directly onto the ballistic protection is affected by the total deflection of the armor, even if the armor
363 deformation itself is lowered after the impact

364 3.3.2 Dyneema® back-packing analysis

365 The damage and penetration of the projectile into the back-packing were analyzed in all the impact
366 points (see Fig. 17):

- 367 ✓ The breakage of the fibers at the point of impact is defined by a square geometry having a
368 constant size of the order of 3 cm for all the impact points.
- 369 ✓ The entrance hole of the bullet presents a cylindrical geometry and a constant diameter inside
370 the target. In the case of complete penetration, the bullet penetrates generating a cylindrical
371 rupture of constant diameter, while for the panels which have retained the bullets penetrations
372 assume a different configuration with a geometry that is not constant and with apparent signs
373 of burning in the internal fibers.
- 374 ✓ Inside the point of impact, the fibers appear to be completely burned and damaged as a result
375 of the penetration of the projectile inside the panel.
- 376 ✓ The damage area on the front of the panel extends on average for a circular area having a
377 diameter of 9-10 cm.
- 378 ✓ The penetration of the projectile inside the panel causes a localized damage, small in size
379 compared to the damage caused on the upper ceramic layer; also the damage is caused only
380 within the fibers and not on the surface layer.



381
382

Fig. 17: Penetration of the bullet from the rear back-packing

383 **4 Numerical simulation**

384 **4.1 Introduction**

385 The numerical methods used for the solution of the ballistic problems involve finite difference, finite
386 volume and finite element approaches as well as meshless approaches. The choice of the applied
387 method depends on the physical nature of the problem being studied, see (Grujicic, et al., 2006a).

388 For numerical simulations of the ballistic problem, the software available to the company OTO
389 Melara is the explicit dynamic solver Ansys-AUTODYN[®], which allows modeling the non-linear
390 dynamics of solids, fluids, gases and their interactions suitably selecting one or more of the above
391 mentioned approaches. This software was found very appropriate for the simulation of high-speed
392 impacts, both for antiballistic impacts and for hyper-speed impacts typical of space debris.

393 The solution of the explicit dynamics allows simulating the mechanical behavior of nonlinear
394 structures during physical events occurring in very short time, approximately a few milliseconds or
395 even less. All these events are dominated by transient behavior of stresses and strains. The main
396 characteristics of the materials are defined by constitutive equations and kinematic equations that
397 describe the dynamic behavior and interactions between strains, stresses and the whole energy of the
398 involved materials. The explicit dynamic simulation is partially implemented and developed as
399 Hydrocodes or SPH (Smoothed Particles Hydrodynamic) codes. In particular, the projectile is defined
400 by SPH particles while the armor system is FEM simulated. The so-called “Hydrocodes” offer an
401 interesting alternative approach to large deformation problems since the lack of a grid removes the
402 need for unphysical erosion algorithm; they are typical dynamic software, particularly suited for
403 modeling impact, penetration and blast events (Clegg, et al., 1996).

404 Additional methods are available in the solver AUTODYN[®]: e.g. it is possible to select among
405 different types of traditional finite element discretization of the problem according to the Lagrangian
406 scheme, the Eulerian scheme, and the arbitrary Lagrangian - Eulerian (ALE) approach, in addition to
407 the discretization of continuum particles through the SPH method.

408 The discretization of solid continuum and structures in the explicit dynamic physic usually takes place
409 through a Lagrangian calculation scheme, in which each body is discretized in a mesh of fixed
410 elements (body fitted mesh), integral with the modeled solid. The Lagrangian solution approach is
411 the most efficient and accurate solution for almost all structural models. However, being the mesh
412 fitted in the modeled solid, large deformation may lead to distorted elements and numerical
413 instabilities. The SPH method is a relatively new mesh-free modeling technique, developed to solve
414 the limitation of the finite element method due to excessive distortion of the mesh. The major
415 advantage of this technique appears to be the lack of numerical grid required for the calculation of
416 the spatial derivatives. It does not entail the use of an unphysical erosion algorithm for the removal
417 of highly distorted grids to help the numerical procedure convergence (Grujicic, et al., 2006a).

418 **4.2 Numerical model**

419 Following the results obtained from previous simulations and experience gained during the research
420 activity reported in (Sabadin, et al., 2014), it was decided to apply a new modeling strategy. The
421 model was developed through a three-dimensional modeling (3D) that allows assessing more
422 accurately the deformation and breakage of the bullet materials and, at the same time, the propagation
423 of cracks and fractures in the ceramic material and the deformation of the rear fibers of Dyneema®.
424 The availability of adequate computing power and the ability to parallelize the simulation on all
425 processors in the available workstations allowed obtaining the computations in reasonable time.
426 The geometry of the bullet and the target permit to reduce the total element number due to their
427 axisymmetric geometry, modeling only a quarter of the projectile and of the target and properly
428 setting the symmetry conditions on the edge surfaces of the target.

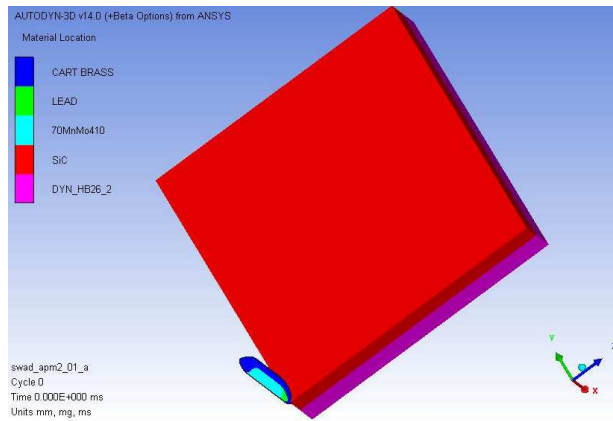


Fig. 18: Geometry of the whole numerical model

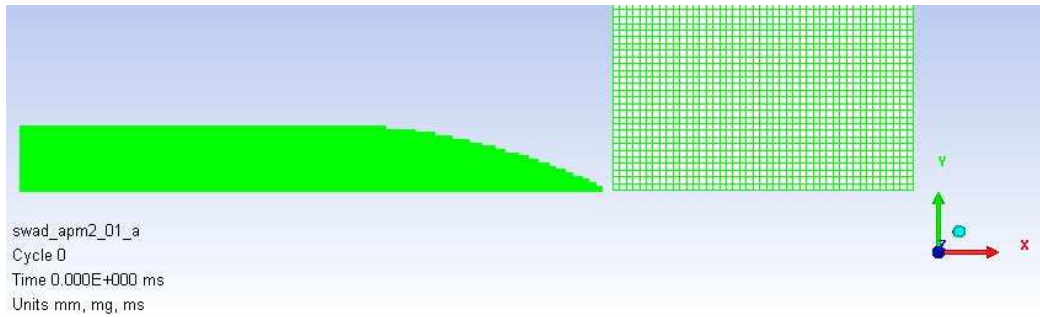
429
430

431 It was also chosen to model the entire bullets using SPH elements: this choice was dictated by the
 432 need to obtain an accurate simulation of the failure behavior of the projectile during the panel
 433 penetration. By using Lagrangian elements, in fact, plastic deformations of the core part of the bullet
 434 was reported that does not properly match the experimental results. By using the SPH elements it is
 435 possible to estimate both the deformation of the projectile inside the panel and the dispersion of the
 436 metal fragments produced during the erosion of the ceramic layer. Moreover, symmetry conditions
 437 can be correctly defined in SPH simulations by suitably defining the simulation domain boundaries
 438 and appropriate conditions for particles in way.

439 As regards the target, instead, it was preferred to use more traditional Lagrangian finite elements.
 440 Both, the static and dynamic mechanical properties of the materials are well defined as far as previous
 441 simulations already provided excellent results for this modeling strategy. It was already proved in
 442 (Sabadin, et al., 2014) that by using common Lagrangian elements it is possible to easily evaluate the
 443 propagation of fractures in the ceramic layer as the penetration of the projectile takes place thanks to
 444 appropriate erosion algorithms. However, the modeling of the rear backpacking material with
 445 Lagrangian elements was rather challenging since the dynamic mechanical properties of Dyneema®
 446 are not easy to assess. Recently, (Lassig, et al., 2015) suitably described the behavior of Dyneema®
 447 laminates by means of Lagrangian elements and therefore reference was made to this pioneering
 448 work. In this case, symmetry conditions should be carefully defined in all layers of the finite element
 449 model also considering transient deformation behavior on symmetry planes.

450 The numerical model simulation is eventually defined by 311,536 elements, among which 40,064 are
451 SPH particles elements and a total of 271,472 are Lagrangian elements.

452 The main dimensions of the bullet and target geometry implemented in the model are reported in Fig.
453 19, where the discretization of their volume is also shown. To proper modeling the bullet geometry
454 and the position of the different materials, particular attention was paid in the model definition.

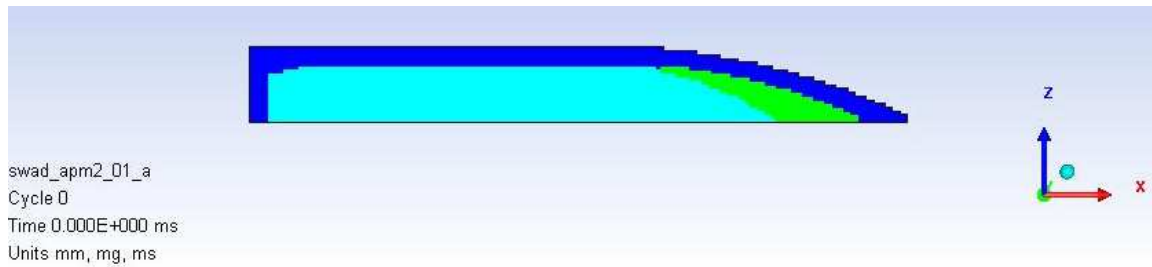


455
456 *Fig. 19: Model geometry and mesh subdivision*

457 4.2.1 Bullet geometry

458 As mentioned, the modeled threat is the cartridge caliber 30-06 SPRG M2. In the simulation, only
459 the geometry of the bullet is defined: the bullet is made of three different materials, a central core
460 made of high hardness steel with a lead tip, all covered by a copper alloy outer jacket. The mechanical
461 materials properties are chosen from the AUTODYN[®] internal library.

462 The bullet has a total length of 35.1 mm and a maximum outer diameter of 7.77 mm. The core
463 geometry is an important part of the bullet, governing the penetration mechanism inside the target
464 panel. A total of 40,064 SPH particle elements were used in total for the definition of the projectile,
465 having each an outer diameter of 0.1 mm (initial distance from other particles). The bullet mesh size
466 was selected after a careful sensitivity analysis and it is deemed optimal to highlight the materials
467 failure behavior and the deformation of all the individual components of the projectile. 17,369
468 elements form the outer jacket brass (dark blue), 20,629 elements the high hardness steel core (blue)
469 and, finally, the lead cap is defined by 2,066 elements. Mechanical properties of each material are
470 described by equations describing the interaction among particles and with domain boundaries.

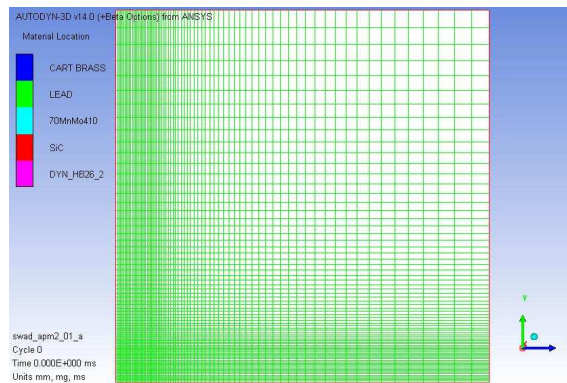


471
472 *Fig. 20: Bullet mesh subdivision*

473 4.2.2 Target Geometry

474 Two different rigidly connected composite materials make up the target panel: for this reason two
475 different groups of three-dimensional Lagrangian finite elements were defined, one for the ceramic
476 layer and one for the rear back-packing, whose geometry was modeled considering the layers'
477 properties and thickness using layered shell finite elements as available in the software.

478 The target model is constituted by three-dimensional elements fitted into a 100 mm square of variable
479 thickness subdivided as shown in Fig. 21. The element size was evaluated based on experimental
480 results and represents the minimum target amplitude that allows assessing the whole extension of the
481 rear bulge resulting after the penetration of the projectile. Furthermore, with this element size, the
482 breakage of ceramic tile surrounding the point of impact can be estimated.



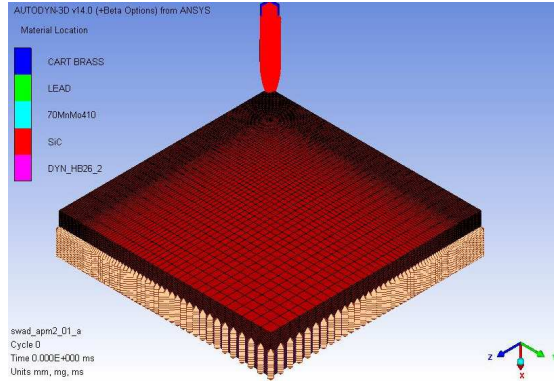
483
484 *Fig. 21: Target mesh discretization*

485 To decrease the total elements number in the model, only 75 elements on each side of the target were
486 used, with variable length size. The element density of the target geometry was refined in the
487 surrounding area of the bullet impact point, thus creating a non-uniform mesh, as shown in Fig. 21.

488 Symmetry boundary conditions were applied on layered shell elements

489 **4.3 Simulation parameters setting**

490 The key parameters for proper simulation configuration of the bullet impact on the target are
491 described in the following. It is assumed that the projectile hits the target at a specific initial velocity
492 while the target composite layer edges are fully constrained.



493
494

Fig. 22: Boundary conditions definition

495 The boundary conditions are applied to the end nodes of the rear part of the target geometry (i.e. the
496 edge of the back surface), in particular by imposing null velocity (and displacements) values in all
497 directions (i.e. Degree of Freedom, DoF) of the nodes of the Dyneema[®] fibres. It means that the
498 bottom of the composite surface edges of the target geometry is completely constrained but the edge
499 surfaces of the ceramic layer are left free as shown in Fig. 22. The bullet initial velocity was also
500 defined, this speed is assumed constant on all the SPH elements of the bullet: a constant speed of
501 about 850 m/s, along the X axis which represents the average speed of experimental ballistic impact,
502 was imposed. Different parts of the model were joined together by appropriate constraints available
503 in the software environment. If two parts are joined, the software automatically identifies and joins
504 all DoF of coincident nodes of the two distinct parts (ANSYS, 2010). The loads and relevant boundary
505 conditions are therefore properly transferred between elements having different characteristics, in this
506 case between the ceramic layer elements and the fibers package elements.

507 The duration of the numerical simulation and the time step are key parameters of the simulation. The
508 following values were found satisfactory for the captioned case: 1,000,000 steps of 0.2 ms each. These
509 values were found to be consistent with the duration of target penetration and with the maximum
510 number of cycles necessary for the development of the entire three-dimensional simulation. In certain

511 simulations, it was subsequently decided to increase the value of the time step bringing it up to a
512 maximum of 0.25 ms in order to obtain a larger amount of information on the deceleration of the
513 projectile inside the target simulating a longer event. To reduce the computational cost, it was decided
514 to set a maximum element speed equal to 20,000 m/s. This setting results in the deletion of the SPH
515 elements that, after the panel impact, become fragments and greatly increase their speed but they are
516 no longer useful for the purposes of the simulation, i.e. the penetration of the projectile, so reducing
517 the computation costs.

518 **5 Material characterization**

519 The used dynamic solver allows implementing the behavior of materials subjected to high dynamic
520 loads through appropriate constitutive models. The material models definitions were implemented
521 into separate set of equations as follows (ANSYS, 2010):

- 522 ✓ Equation of State: define the relation between the hydrostatic pressure, the local density and
523 local specific energy of the material.
- 524 ✓ Strength equation: describes the materials behavior, in particular the deformation during the
525 high dynamic loads application. Basically, the stress-strain relationships are set.
- 526 ✓ Failure mode: simulate the various ways in which materials fail under extreme loading
527 conditions, resulting in crushed or cracked materials, considering the above mentioned set of
528 equations and relevant variables.
- 529 ✓ Erosion algorithm: it is a numerical mechanism for the automatic removal (deletion) of
530 elements during a simulation. Erosion can be used to allow the simulation of material fracture
531 and penetration, removing very distorted elements before they degenerate. The stresses
532 associated to deleted nodes are transferred to remaining nodes.

533 While dynamic characterization of other materials is available i (ANSYS, 2010) n, the ballistic
534 impact simulation on composite Dyneema® has been possible thanks to an intensive literature survey
535 aimed at finding dynamic mechanical properties of this composite material.

536 **5.1 Metallic materials**

537 For metallic materials considered in the numerical simulation such as steel, lead and brass a simple
538 linear equation of state linking pressure and internal volume variations is used:

539 $P = K\mu$ Eq. 1

540 Where : $\mu = \frac{\rho}{\rho_0} - 1$ is the compression coefficient, being ρ_0 the initial density, ρ the current density,
541 and K the bulk modulus. To represent the constitutive response of metallic material models subjected
542 to deviatoric strains it is used the model of Johnson-Cook presented in (Johnson & Cook, 1983).
543 Reference was made to data of a steel alloy, made available from prior research by OTO Melara. This
544 material is described by a "shock" equation of state (EoS); the stiffness is provided according to the
545 Johnson-Cook equation.

546 The mechanical properties of the materials used for the cap, namely brass and the lead, have been
547 selected in the software material library: considering the experience gained in the simulation of
548 dynamic impacts, the two materials guaranteed good numerical results. Cartbrass material was
549 exterior brass defined through a "shock" EoS and again by Johnson Cook constitutive model, while
550 the lead material used for the inner part was defined by a "shock" EoS and a different constitutive
551 model, defined by Steinberg Guinan strength equation (Steinberg, 1991).

552 The a.m. metallic materials are used to characterize SPH particle elements, so they do not require an
553 erosion algorithm to allow the correct simulation performance, removing mesh elements too distorted:
554 this allows obtaining a more accurate simulation regarding the bullet damage inside the target and the
555 fragments propagation generated during the ogive erosion.

556 **5.2 Ceramic material**

557 To describe the mechanical behavior of the ceramic materials, particularly of the SiC layer, a
558 polynomial EoS is used in which the relationship between pressure, density and value of internal
559 energy is set considering the intact model. Inside the ceramic materials, when the damage begins to
560 occur due to the action of external loads, it is possible to have bulking phenomena. The effect of
561 bulking occurring in brittle materials is to increase the internal pressure while keeping constant the

562 volumetric density and/or increase the volumetric strain, maintaining constant the pressure. For the
563 full definition of Johnson-Holmquist constitutive equations and damage model, reference was made
564 to the implementation of this relation in (Holmquist & Johnson, 2005).

565 The SiC ceramic material model available in the Autodyn[®] materials library is used in all the
566 simulations. The constitutive properties and the damage equations are defined by the JH-1 Johnson-
567 Holmquist equation. The description of the ceramic materials through Johnson-Holmquist equations
568 implementation is known to be correct and of common use in the simulation of dynamic events.

569 In addition to the dynamic mechanical properties of the material, the so called "instant" erosion
570 algorithm was also defined, being Lagrangian elements still applied (ANSYS, 2010). These
571 equations were set after careful sensitivity analyses. In particular, the Geometric Strain erosion model
572 is used in this work, and the maximum geometric strain of each individual element is computed
573 according to all the strain components.

574 **5.3 Orthotropic material**

575 Specific attention was paid to the mechanical characterization of Dyneema[®] fiber reinforced
576 laminates, in our case of the Dyneema[®] Hard Ballistic 26 fibers. In the software library, the physical
577 parameters of such innovative material are not reported: in fact it was manufactured and in use for
578 production of ballistic protections only recently and, understandably, confidential in commerce.

579 These parameters are difficult to find out but actually several mathematical models for defining
580 Dyneema[®] behavior were developed and applied in the earlier stages of the research. The model
581 presented by (Grujicic, et al., 2006a), partially provides the necessary parameters for Dyneema[®] fibers
582 description in the software and the Dyneema[®] BT-10 mathematical model previously applied by OTO
583 Melara in other studies may be adapted for the purpose. However, these mathematical models do not
584 guarantee the correct simulation of the Dyneema[®] Hard Ballistic 26 behavior: in facts, the results
585 obtained in preliminary computations are not in agreement with the experimental results of the
586 ballistic tests.

587 Very recently, it has been published a comprehensive paper related to the main values of the
588 mechanical properties of the Dyneema® Hard Ballistic 26 laminate definition (Lassig, et al., 2015).
589 The paper provides results of laboratory tests carried out for the numeric parameter validation and
590 presents numerical values of the individual parameters necessary for material implementation.
591 Such material behavior is much more complex than a traditional isotropic constitutive model used in
592 anti-ballistic field. Additional effects to complete the material model include:

- 593 ✓ Anisotropy properties of the stiffness matrix of the material;
- 594 ✓ The tensile strength/stiffness decrease due to anisotropy and the post-failure behavior of the
595 damaged material;
- 596 ✓ The relationship between the spherical and deviatoric component of the stress tensor;
- 597 ✓ The non-linearity effect in the pressure and density relationship.

598 Fiber composite materials mechanical responses subject to large deformations and high strain rate are
599 defined through the orthotropic material model defined by Clegg (Clegg, et al., 1999). This material
600 is based on the original idea proposed in (Anderson, et al., 1994), where Authors developed a
601 theoretical approach to the material anisotropy coupling it with the nonlinear material response.

Orthotropic linear elastic model			Effective stress-strain σ - ϵ values			Plasticity Coefficients			Effective stress-strain σ - ϵ values				
E ₁₁	3.62	[Gpa]	$\sigma_{eff\#1}$	1.76E+02	[kPa]			Unit			Unit		
E ₂₂	26.9	[Gpa]	$\sigma_{eff\#2}$	9.89E+02	[kPa]	a ₁₁	3.00E-02	[-]	σ_{11fail}	1.07	[Mpa]		
E ₃₃	26.9	[Gpa]	$\sigma_{eff\#3}$	1.74E+03	[kPa]	a ₂₂	1.00E-05	[-]	σ_{22fail}	753	[Mpa]		
ν_{12}	0.013	[-]	$\sigma_{eff\#4}$	2.42E+03	[kPa]	a ₃₃	1.00E-05	[-]	σ_{33fail}	753	[Mpa]		
ν_{23}	0	[-]	$\sigma_{eff\#5}$	3.10E+03	[kPa]	a ₁₂	1.00E-06	[-]	τ_{12fail}	1.01E+20	[Mpa]		
ν_{31}	0.5	[-]	$\sigma_{eff\#6}$	5.97E+03	[kPa]	a ₁₃	1.00E-06	[-]	τ_{23fail}	35.2	[Mpa]		
G ₁₂	30.7	[Mpa]	$\sigma_{eff\#7}$	1.20E+04	[kPa]	a ₂₃	1.00E-06	[-]	τ_{31fail}	1.01E+20	[Mpa]		
G ₂₃	42.3	[Mpa]	$\sigma_{eff\#8}$	2.07E+04	[kPa]	a ₄₄	1.00	[-]	G _{c11}	790	(J/m ²)		
G ₃₁	30.7	[Mpa]	$\sigma_{eff\#9}$	3.46E+04	[kPa]	a ₅₅	1.75	[-]	G _{c33}	30	(J/m ²)		
Polynomial EOS			$\sigma_{eff\#10}$	2.02E+08	[kPa]	a ₆₆	1.75	[-]	G _{c22}	30	(J/m ²)		
A ₁	7.04	[Gpa]	$\epsilon_{eff\#1}$	1.82E-04	[-]				G _{c31}	1.46	(J/m ²)		
A ₂	10	[Gpa]	$\epsilon_{eff\#2}$	1.20E-03	[-]				G _{c12}	1.46	(J/m ²)		
A ₃	0	[Gpa]	$\epsilon_{eff\#3}$	3.11E-03	[-]				G _{c23}	1.46	(J/m ²)		
B ₀	3.864	[-]	$\epsilon_{eff\#4}$	6.92E-03	[-]				Damage Coupling	0.5	(kPa)		
B ₁	3.864	[-]	$\epsilon_{eff\#5}$	1.13E-02	[-]								
T ₁	7.04	[Gpa]	$\epsilon_{eff\#6}$	2.83E-02	[-]								
T ₂	0	[Gpa]	$\epsilon_{eff\#7}$	5.78E-02	[-]								
T _{ref}	293	[K]	$\epsilon_{eff\#8}$	1.06E-01	[-]								

Specific Heat	1850	[J/kgK]	$\epsilon_{eff\#9}$	1.061E-01	[-]
Thermal Cond.	0	[J/mKs]	$\epsilon_{eff\#10}$	1	[-]

Table. 6 Dyneema® Hard Ballistic 26 mechanical properties (Lassig, et al., 2015)

602

603 Regarding the fibrous composites, the main causes of failure due to impact loads, are identified as the
604 delamination between the layers, the shear deformations causing the matrix failure, and the fibers
605 failure themselves. These failure modes lead to a reduction of the ability to sustain a load in one or
606 more directions and for this reason, this phase as well as that of softening, i.e. the reduction of the
607 ability to support tensile stress during deflection, was considered. Other failure modes are due to the
608 matrix fusion ("burning") and fibers degradation due to an excessive thermal gradient in the material:
609 these effects are taken into account only in hypervelocity impacts while they are not relevant for
610 impacts with speeds lower than 1000 m/s, as in this case.

611 **6 Results of the numerical simulations**

612 All the results obtained from the numerical simulations carried out of 7.62 caliber M2 bullet impacts
613 on antiballistic composite advanced protections are reported in the following. The obtained results
614 overview allows evaluating mathematical and physical parameters optimization carried out in the
615 present research, aimed at obtaining a numerical model able to simulate the experimental results. The
616 results of each simulation are shown in Table 8 to Table 10 and the differences are highlighted to
617 properly understand the numerical results obtained. As a conclusion, a comparison between the
618 numerical solution and the experimental values is presented.

619 **6.1 Simulations analysis**

620 From the nine numerical simulations conducted using three-dimensional Lagrangian and SPH
621 elements, remarkably interesting results were obtained. The numerical parameters that most influence
622 the result of the simulation are reported in Table 7 showing the used values in each simulation
623 normalized with respect to reference values. For each simulation, reference values of the materials
624 mechanical characteristics used for the Dyneema® definition are shown: the index 1 refers to the

625 parameters reported in (Lassig, et al., 2014), while index 2 means the materials mechanical
 626 description given by (Lassig, et al., 2015).

627 Simulation no. 8 represents the best numerical solution in which the most suitable numerical results
 628 in term of bullet arrest and rear panel deformation were achieved: the combination of correct
 629 thicknesses of the materials used, model geometry definition and Dyneema® mechanical
 630 characterization allowed to obtain excellent results.

MAIN PARAMETERS						
Simulation	Dyneema® material	Dyneema® Erosion	Dyneema® Thickness	Ceramic erosion	Ceramic Thickness	Target items
[n°]	-	[%]	[%]	[%]	[%]	-
0	1	1.5	-	1.5	-	2
1	2	1.5	-	1.5	-	2
2	2	1.5	-	1.5	-	4
3	1	1.5	-	1.5	-12.5%	2
4	1	1.5	-30.0%	1.5	12.5%	2
5	1	1.5	-	1.5	-	1
6	2	1.5	-	1.5	-	1
7	2	2	-	2	-	2
8	2	2	10.0%	2	-	2
9	2	1.5	10.0%	2.5	-	2

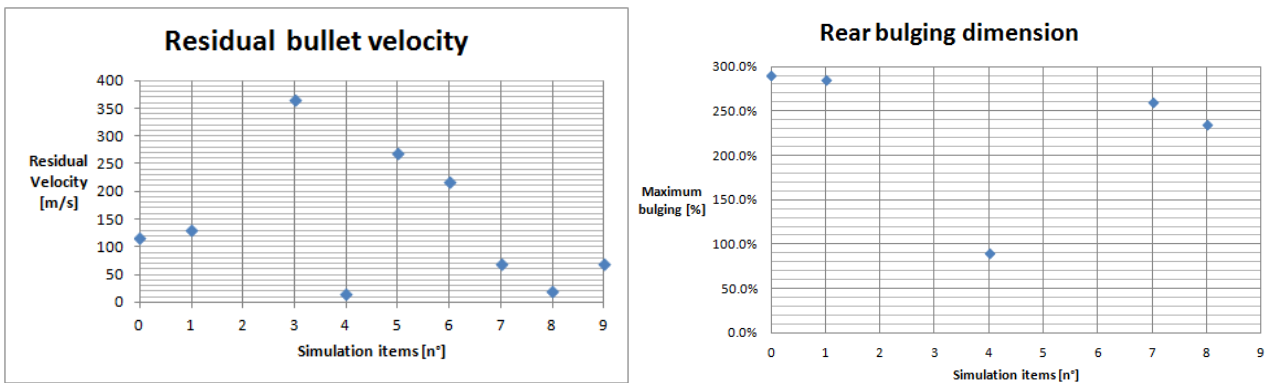
631 *Table. 7 Main simulation parameters*

632 In simulation no. 4 the material layer thicknesses were changed to verify the possibility of future
 633 development of the ballistic protection: indeed the simulation increasing the ceramic layer thickness
 634 and decreasing the Dyneema® one showed a remarkable improvement in term of maximum rear
 635 bulging extension due to the thickness change.

SIMULATION RESULTS					
Simulation	Simulation Time	Bullet penetration	Residual Velocity	Maximum bulging	Damage extension
[n°]	[ms]	-	[m/s]	[%]	[%]
0	0.25	YES	116	290.0%	240.0%
1	0.2	YES	132	285.0%	200.0%
2	0.09	YES	/		/
3	0.16	YES	365		/
4	0.17	NO	-	90.0%	200.0%
5	0.2	YES	270		/
6	0.2	YES	217		/
7	0.22	YES	70	260.0%	240.0%
8	0.22	NO	-	235.0%	230.0%
9	0.22	YES	70		/

636 *Table. 8 Main simulation results (bulging measured in one panel only)*

637 From the results reported in Table 9, it is clear that only the simulations no. 4 and 8 reach the almost
 638 complete bullet stop inside the amour protection: it is impossible to confirm that the complete bullet
 639 stop is reached in the simulation due to numerical difficulties preventing the conclusion of the
 640 numerical calculation. Thus, not allowing to get the desired result. In Fig. 23, the residual velocity
 641 and bulging maximum values for each simulation are shown: the smaller values of residual velocity
 642 are found for simulations no 4 and 8, being less than 2% of the initial bullet velocity. Simulation no
 643 4 gets a significantly reduction of the rear bulging, that is expressed in percentage of the armor total
 644 thickness, instead the damage extension is referred to the ceramic tile dimension.



645
 646 *Fig. 23: Residual velocity and maximum rear bulging*

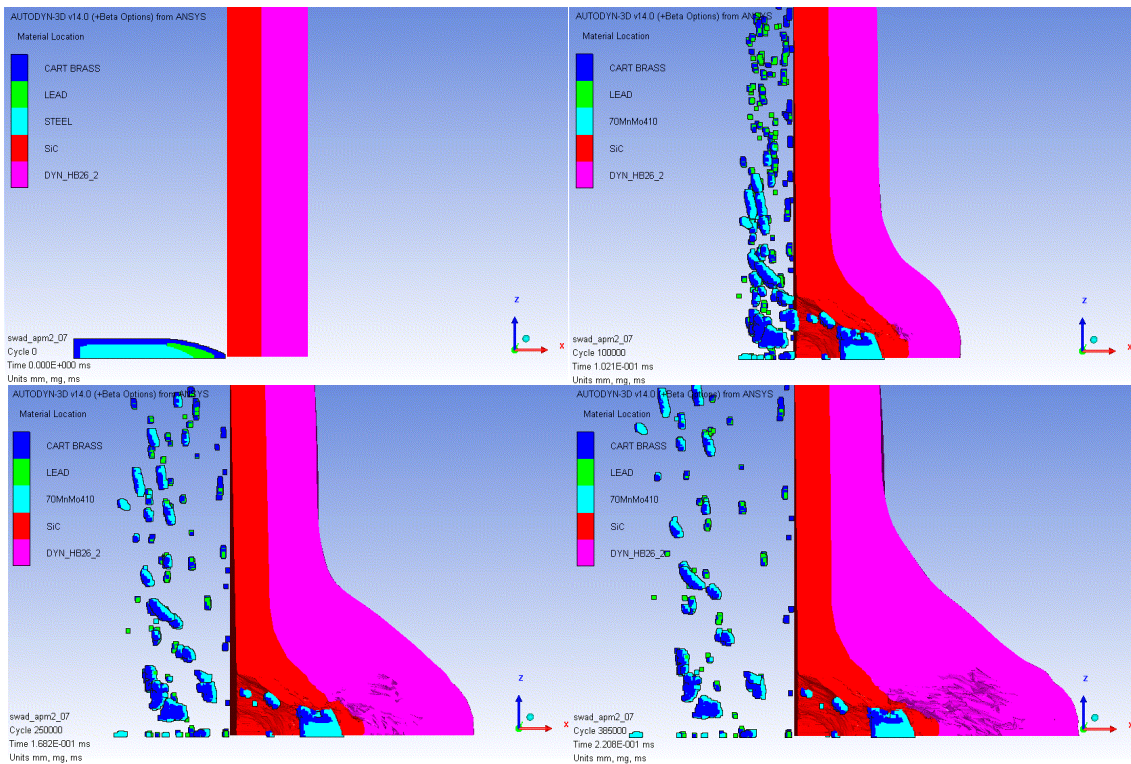
647 The process conducted during this research phase has therefore resulted in an overall improvement
 648 of the geometry and of the results derived from numerical simulations: a good approximation of the
 649 ballistic tests results with regard to the bulging deformation and the extension of the ceramic cracking
 650 was obtained. Images of Fig. 24 show the rear panel deformation and the entrance hole of the bullet
 651 on the ceramic layer.

652 **6.2 Numerical simulation validation**

653 The numerical model used in the simulation provides elements bonding between two distinct stacked
 654 layers, ceramic and rear fibers. Compared to previous simulations the erosion value is changed in
 655 both materials: the geometric strain erosion is set equal to 2.0, i.e. allowing each element a maximum
 656 volumetric deformation equal to 200% of the initial dimension (before removing the element from

657 the numerical simulation). The elements are more deformed thus absorbing more initial energy during
658 bullet penetration. In Fig. 24, the penetration sequence in to the armor protection is reported.

659



660

661

Fig. 24: Bullet penetration sequence

662 Data of greatest interest in the model are the bullet velocity decrease inside the target: as shown in
663 Fig. 25, the gauge point speed in the rear area of the projectile decreases significantly, reaching at
664 time $t=0:22$ ms the speed of 20 m/s.

665

666

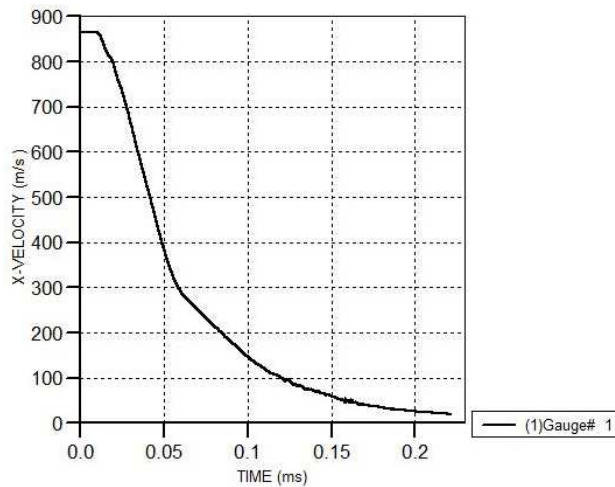
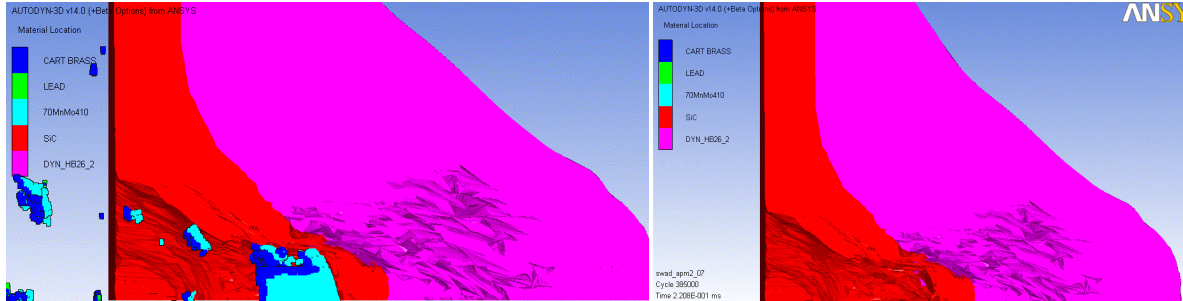


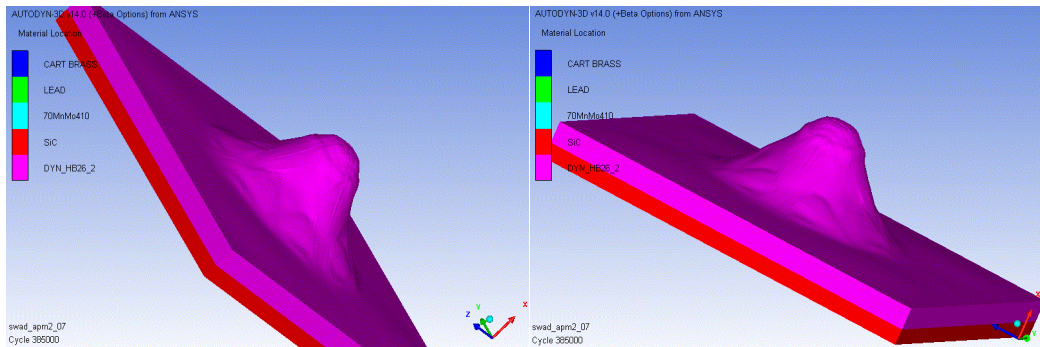
Fig. 25: Projectile velocity diagram

667 The residual speed of 20 m/s results to be 2.3% of the initial bullet velocity, so the numerical model
668 is validated as it predicts a complete stop of the bullet inside the target and does not cause any rear
669 pull-out fragments phenomena of composite material as measured in the tests.



670
671 *Fig. 26: Zooming on the point of impact*

672 From Fig. 26, it is possible to evaluate the maximum deflection of the rear package and the diameter
673 extension of the damaged area . The damage in the simulations is the maximum dynamic extension
674 due to the high velocity impact. Finally, it can be stated that the choice of increasing by 10% the
675 fibers layers thickness is correct for obtaining results in agreement with the experimental tests already
676 carried out. The numerical three-dimensional images allow a first qualitative comparison with the
677 experimental tests images (see Fig. 27 in comparison to Fig. 11 and Fig. 13).

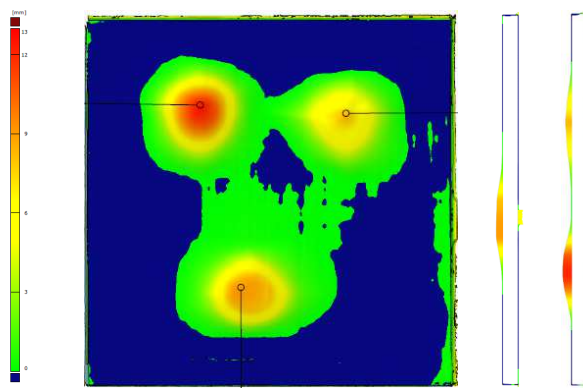


678
679 *Fig. 27: Tri-dimensional simulated damaged area*

680 **6.3 Numerical and experimental results comparison.**

681 Particular attention was paid to the maximum value of bulge deflection, as very significant to assess
682 the rear damage produced by the threat. During ballistic tests, authors managed to evaluate both the
683 static damage due to the impact, the maximum value of the rear bulge after impact, and the dynamic
684 damage in terms of maximum deflection in the transient dynamic phase using modeling clay. From
685 the three-dimensional scans carried out on composite panels, the maximum value of the static

686 deflection of each panel and the rear damage extension, specifically its maximum size, was assessed.
 687 These values were then compared to those obtained experimentally through destructive analysis in
 688 which the panels were analyzed in order to understand the damage mechanisms of each materials and
 689 the real damage dimensions due to the bullet impact. In Fig. 28, the three-dimensional scanning of
 690 the rear face of the composite panel and the perpendicular sections to the impact plane are shown. On
 691 both images, the areas that present rear deflection values greater than 1 mm and the maximum values
 692 of the deflection measured at the impact point are highlighted. These values are significantly lower
 693 than those measured after the tests on the clay. Indeed, measured values do not exceed about 10-12
 694 mm for all measured specimens while during the tests they deform much more at impact instant and
 695 then return in a final static deformed configuration.



696
697 *Fig. 28: Tri-dimensional scan of a panel*

698 The values for the three impacts on the specimens in term of maximum rear bulging, damage
 699 extension on the front of the fibers package and rear deflection area extension measured directly on
 700 the back-packing are summarized in Table 10 in normalized format.

Numerical and Experimental results comparison							
Panel and simulations	n° hole	Bulging	Est. Damage Penetration		Est. Bulge Propagation		Internal
			HOR.	VERT.	HOR.	VERT.	Penetration
	n°	[%]	[%]	[%]	[%]	[%]	[%]
SiC & Dyneema®	1	41.0%	62.0%	68.0%	248.0%	238.0%	105.0%
	2	62.0%	64.0%	76.0%	268.0%	288.0%	130.0%
	3	45.0%	62.0%	74.0%	274.0%	256.0%	110.0%
Simulation 8	1	235.0%	66.0%	66.0%	260.0%	260.0%	155.0%

701
702 *Table. 9 Damage size on impacted panels*

703 Then, the numerical and experimental results are compared and commented as follows:

704 ✓ Bulging: the maximum bulging value measured in the simulation turns out to be considerably
705 greater than the static value measured after the tests. This discrepancy occurs because of the
706 simulation time: the numerical simulation was stopped after 0.2 ms after the impact contact,
707 i.e. during the dynamic transient phase of the penetration. The numerical bulging is therefore
708 more in agreement with the real dynamic deflection measured on the clay. Namely, the clay
709 average deflection measured a rather large penetration in the rear armor plate, about 3 times
710 the static one. The numerical damage seems to be slightly higher than this value because of
711 the back-clay layer absence in the simulation, certainly affecting the total panel deformation.
712 To obtain comparable values a longer numerical simulation, at least of a few milliseconds, is
713 needed. This would imply more computational time to run a single simulation and,
714 consequently, more computational power.

715 ✓ Penetration damage defines the fibers rupture dimensions due to the impact in the front part
716 of the armor panel. These numerical values are in good agreement with the experimental
717 penetration values measured on the panels: the average experimental results to be in the order
718 of a few millimeters, which differ by 2.4% from the value determined in the numerical
719 simulation. Therefore, the numerical bullet hole in the fiber layer seems to reproduce correctly
720 the real penetration size of the projectile inside the composite target.

721 ✓ Bulge propagation: the average extension of the rear bulging measured during the
722 nondestructive test is of the order of 10 -15 cm, less than 1% from the simulation result.

723 ✓ Bullet penetration in the numerical model results to be 35% higher than the average
724 penetration measured experimentally on the impact panels. However, the measurements are
725 quite difficult to perform even during destructive test. Considering the difficulties to define
726 the real damage and the uncertainty affecting the real numerical penetration values, this
727 comparison can be considered as a good indication but it does not represent a fully satisfactory
728 information.

729 In general, the obtained numerical simulation results are satisfactory to define the complete stop of
730 the bullet into the target and the obtained model can be used to optimize the layer thicknesses of the
731 armor. Moreover, the obtained results also confirm a good degree of accuracy in the damage extension
732 description for both the front and rear parts of the panel.

733 **7 Conclusions**

734 This work presents the development and validation of a numerical model for the simulation of high
735 velocity impact on advanced composite armor systems. Combining both mesh and meshless
736 approaches, a highly refined numerical model was developed in the ANSYS-Autodyn® environment.
737 An armor system made up by a first layer of SiC ceramic glued onto a back-packing made of
738 UHMWPE laminate, was considered. Due to the lack of experimental and numerical results in
739 literature concerning this impact typology, a parallel experimental campaign was conducted in order
740 to validate the numerical results: three rectangular add-on panels were built, aimed at providing the
741 fourth protection level (named Armor-Piercing Rifle) as defined by the NIJ Standard 0108.01
742 (National Institute of Justice, 1985). Namely, the level of threat considered is a 30-06 M2 Armour
743 Piercing (AP) bullet.
744 On each panel, three M2 bullets were fired in points marked in correspondence of the SiC tiles. Once
745 completed the experimental tests, non-destructive and destructive analyses were carried out on the
746 panels, aimed at obtaining the characterization of the different types of damage and fractures due to
747 the impact into ceramic material and into back-packing. These analyses also allowed displaying and
748 defining the actual mechanism of penetration of the projectile inside the composite material.
749 In conclusion, the comparison reveals a good agreement between experimental and computational
750 results in terms of ballistic properties, deformations, fragmentation and fracture of the ballistic armor
751 system. Such experimental/numerical comparison allows validating the numerical strategy adopted
752 by the authors.

753 **8 Acknowledgements**

754 The work has been partially funded by the research grant DPU12UNIGE82/6100 of Regione Liguria,
755 Italy (Fondo Sociale Europeo Regione Liguria 2007-2013 Asse IV “Capitale Umano” ob.specifico
756 I/6).

757 **9 References**

- 758 Anderson Jr., Ch.E., Cox, P.A., Johnson, G.R., Maudlin, P.J. 1994 A constitutive formulation for
759 anisotropic materials suitable for wave propagation computer programs-II. *Computational*
760 *Mechanics*, 15 (3), pp. 201-223.
- 761 ANSYS, 2010. *Ansys Help System*. s.l.:ANSYS.
- 762 Clegg, R., Hayhurst, C., Livingstone, I. & Francis, N., 1996. *The application of SPH techniques in*
763 *Autodyn-2D to ballistic impact problems*. San Francisco/CA, USA, s.n.
- 764 Cunniff, P., 1999. *Dimensionless parameters for optimization of textile-based body armor systems*.
765 San Antonio, Texas, Technomic Publishing, Lancaster Pennsylvania, pp. 1301-10.
- 766 Fallah, A.S., Micallef, K., Langdon, G.S., Lee, W.C., Curtis, P.T., Louca, L.A. 2014 Dynamic
767 response of Dyneema® HB26 plates to localised blast loading. *International Journal of Impact*
768 *Engineering*, 73, pp. 91-100.
- 769 Fecko, D., Lyle, D. & Xavier, G., 2005. *Composite armor solution for STANAG 4569 ballistic*
770 *protection levels*. Paris, France, SAMPE Europe, pp. Paper SE 05-34.
- 771 Flores-Johnson, E.A., Saleh, M., Edwards, L. 2011. Ballistic performance of multi-layered metallic
772 plates impacted by a 7.62-mm APM2 projectile. *International Journal of Impact Engineering*, 38
773 (12), pp. 1022-1032.
- 774 Forrestal, M.J., Børvik, T., Warren, T.L. 2010. Perforation of 7075-T651 Aluminum Armor Plates
775 with 7.62 mm APM2 Bullets. *Experimental Mechanics*, 50 (8), pp. 1245-1251.
- 776 Frissen, R., 1996. *Modeling the ballistic impact behaviour of polyethylene-fibre-reinforced*
777 *composites*, Eindhoven: Eindhoven University of Technology.
- 778 Grujicic, M., Arakere, G., He, T., Bell, W.C., Cheeseman, B.A., Yen, C.-F., Scott, B. 2008. A ballistic
779 material model for cross-plyed unidirectional ultra-high molecular-weight polyethylene fiber-
780 reinforced armor-grade composites. *Materials Science and Engineering A*, 498 (1-2), pp. 231-241.
- 781 Grujicic, M., Bell, W.C., Thompson, L.L., Koudela, K.L., Cheeseman, B.A. 2008. Ballistic-
782 protection performance of carbon-nanotube-doped poly-vinyl-ester-epoxy matrix composite armor
783 reinforced with E-glass fiber mats. *Materials Science and Engineering A*, 479 (1-2), pp. 10-22.
- 784 Grujicic, M., Pandurangan, B., Koudela, K.L., Cheeseman, B.A. 2006. A computational analysis of
785 the ballistic performance of light-weight hybrid composite armors. *Applied Surface Science*, 253 (2),
786 pp. 730-745.
- 787 Hayhurst, C.J., Hiermaier, S.J., Clegg, R.A., Riedel, W., Lambert, M. 1999. Development of material
788 models for Nextel and Kevlar-epoxy for high pressures and strain rates. *International Journal of*
789 *Impact Engineering*, 23 (1 PART I), pp. 365-376.
- 790 Hogg, P., 2003. *Composites for Ballistic Applications*. London, Queen Mary, University of London.
- 791 Holmquist, T.J., Johnson, G.R. 2005. Characterization and evaluation of silicon carbide for high-
792 velocity impact. *Journal of Applied Physics*, 97 (9), art. no. 093502,

- 793 Iannucci, L., Pope, D. & Dalzell, M., 2009. *A constitutive Model for Dyneema UD composites*.
794 Edinburgh, The British Composites Society, p. 10.
- 795 Johnson, G. & Cook, W., 1983. *A constitutive model and data for metals subjected to large strains,*
796 *high strain rates and high temperatures..* Hague, The Netherlands, s.n., pp. 541-547.
- 797 Karthikeyan, K., Russell, B.P., Fleck, N.A., Wadley, H.N.G., Deshpande, V.S. 2013. The effect of
798 shear strength on the ballistic response of laminated composite plates. *European Journal of*
799 *Mechanics, A/Solids*, 42, pp. 35-53.
- 800 Lässig, T., Riedel, W., Heisserer, U., Van der Werff, H., May, M., Hiermaier, S. 2014. Numerical
801 sensitivity studies of a UHMWPE composite for ballistic protection. *WIT Transactions on the Built*
802 *Environment*, 141, pp. 371-381.
- 803 Lässig, T., Nguyen, L., May, M., Riedel, W., Heisserer, U., Van Der Werff, H., Hiermaier, S. 2015.
804 A non-linear orthotropic hydrocode model for ultra-high molecular weight polyethylene in impact
805 simulations. *International Journal of Impact Engineering*, 75, pp. 110-122.
- 806 C.T. Lim, V.P.W. Shim, Y.H. Ng.2003. Finite-element modeling of the ballistic impact of fabric
807 armor, *International Journal of Impact Engineering*, Volume 28, Issue 1, Pages 13-31
- 808 National Institute of Justice, 1985. *Ballistic Resistant Protective Materials- NIJ Standard 0108.01*.
809 Washington, DC(U.S.A.): U.S. Department of Justice.
- 810 NATO, S. a., 2004. *STANAG 4569 Land (edition 1) - Protection levels for occupants of logistic and*
811 *light armoured vehicles*. Brussels: NATO.
- 812 O'Masta, M.R., Deshpande, V.S., Wadley, H.N.G. 2014. Mechanisms of projectile penetration in
813 Dyneema® encapsulated aluminum structures. *International Journal of Impact Engineering*, 74, pp.
814 16-35.
- 815 Ramadhan, A.A., Abu Talib, A.R., Mohd Rafie, A.S., Zahari, R. 2013. High velocity impact response
816 of Kevlar-29/epoxy and 6061-T6 aluminum laminated panels. *Materials and Design*, 43, pp. 307-
817 321.
- 818 Russell, B.P., Karthikeyan, K., Deshpande, V.S., Fleck, N.A. 2013. The high strain rate response of
819 Ultra High Molecular-weight Polyethylene: From fibre to laminate. *International Journal of Impact*
820 *Engineering*, 60, pp. 1-9.
- 821 Sabadin, G., Bassano, A., Rizzo, C. & Gaiotti, M., 2013. *Modellazione e simulazione d'impatti ad*
822 *alta velocità Report n: 13GSA02*, s.l.: OTO Melara.
- 823 Sabadin, G., Gaiotti, M., Rizzo, C. & Bassano, A., 2014. Optimization of ballistic properties of an
824 advanced composite armor system: analysis and validation of numerical models subject to High
825 Velocity Impacts. In: *Maritime Technology ad Engineering*. Lisbon: C. Guedes Soares, T.A. Santos,
826 pp. 463-475.
- 827 Steinberg, D., 1991. *Equation of State and Strength Properties od Selected Materials*. s.l.:Lawrence
828 Livermore National Laboratories Report.